The extreme acoustic anisotropy and fast sound velocities of cubic high-pressure ice polymorphs at Mbar pressure

Jin S. Zhang (iD), M. Hao (iD), Z. Ren, and B. Chen (iD)

View Online   Export Citation   CrossMark

ARTICLES YOU MAY BE INTERESTED IN

Applied Physics Letters

Mid-IR and THz frequency combs special collection

Read Now!

The extreme acoustic anisotropy and fast sound velocities of cubic high-pressure ice polymorphs at Mbar pressure

Jin S. Zhang,[1,2,a] (iD) M. Hao,[1,2] (iD) Z. Ren,[1,2] and B. Chen[3] (iD)

AFFILIATIONS

[1] Department of Earth and Planetary Sciences, University of New Mexico, Albuquerque, New Mexico 87131, USA
[2] Institute of Meteoritics, University of New Mexico, Albuquerque, New Mexico 87131, USA
[3] Department of Geology and Geophysics, Hawaii Institute of Geophysics and Planetology, School of Ocean and Earth Science and Technology, University of Hawaii at Manoa, Honolulu, Hawaii 96822, USA

[a] Email: Jinzhang@unm.edu

ABSTRACT

We presented the experimentally determined single-crystal elasticity model of ice up to 103(3) GPa, based on the sound velocity measurements of high-P ice polymorphs within multiple diamond anvil cells using Brillouin spectroscopy. We have not observed any discontinuities of the P-wave (V_p) or S-wave (V_s) velocities over the entire P range. The elastic moduli of high-P ice show a close to linear P dependence. In comparison with the high-P silicate minerals in terrestrial planetary bodies, the V_p and V_s values of ice exceed those of both bridgmanite and ferropericlase at $P > 80$–90 GPa, counter-intuitively indicating that the high-P ice, if existing in the deep terrestrial planets' interior, is not a slow phase. Instead, the high-P ice shows extremely strong elastic anisotropy, reaching 27% and 74% at 100 GPa for V_p and V_s, respectively. The presence of high-P ice in terrestrial planets' interior, even on a small scale may lead to the observable anisotropic signatures, such as the 25% V_s anisotropy in the deep earthquake-generating zone in subducting slabs. We anticipate our measurements to serve as an important base for explaining and modeling the geophysical observations for various types of planetary bodies.

Ice is a major component of icy planets, satellites, and explanets,[1–6] and the thermochemical convections of liquid H_2O and its solid high-pressure (P) polymorphs are considered to be responsible for the high magnetic fields of Uranus and Neptune[5] and the possible tectonic activities in Titan and Europa.[3–6] Ice is also a possible minor component in the interior of terrestrial planets like Earth and Mars.[7] Although the form of H_2O is primarily supercritical fluid with dissolved silicates in the Earth's mantle, under cold subduction slab geotherms or within colder terrestrial planetary bodies, H_2O can exist in the form of solid high-P ice polymorphs rather than fluid.[7,8] Therefore, a high-P phase diagram and its thermoelastic properties at high-P conditions are of fundamental importance for Earth and planetary sciences.

Ice shows complicated P-T phase diagrams with more than 15 known crystalline forms.[9] Under room-temperature (T) conditions, ice crystallizes into a disordered molecular phase ice VII at $P > 2.5$ GPa and subsequently transforms into an ordered ionic form ice X at between 40 and 80 GPa.[10–15] Different ice polymorphs are expected to have distinct thermoelastic and optical properties due to varying intra and intermolecular bonding. However, the sharp jumps of the thermoelastic and optical properties across the ice VII to ice X transition remain controversial.[12–21] In particular, theoretical calculations suggest that the ordered ionic ice X has much higher elastic moduli and thus smaller compressibility than its low-P molecular polymorph ice VII,[14,22] which can affect the differentiation and convection of large icy planetary bodies.[1] Both ice VII and ice X are cubic, and such a dramatic change in elastic properties, unfortunately, has not been indubitably observed in previous elasticity measurements.[14,15,17,20,21]

In order to locate the ice VII–X transition boundary and determine the single-crystal elastic properties of ice VII and X, we have performed direct sound velocity measurements on high-P ice polymorphs in multiple diamond anvil cells (DACs) between 4.1(1) and 103(2) GPa using Brillouin spectroscopy. We have used the symmetric DACs with a pair of 350 μm or 300 μm cutlet diamonds for generating high-P conditions. Pre-indented Re foil with a 180 μm or 165 μm hole in the center was used as the gasket. Before loading the de-ionized water, two or three ruby spheres separated ~180° or ~120° from each other were placed inside the DAC sample chamber for measuring the P and evaluating the P gradient. The P increase was slow, and careful

annealing with a hot plate up to $100\,^\circ$C was employed to encourage crystal growth. All the Brillouin spectroscopy experiments were performed at the high-P laser spectroscopy laboratory at the University of New Mexico (supplementary material, Fig. S1). A 532 nm diode-pumped solid-state laser is used as an excitation source at a constant output power of 300 mW, and approximately 50%–60% of the power reaches the sample due to the absorption and/or reflection from the optical elements in the optical path. P values were determined by ruby fluorescence measured using an Ocean Optics HR2000+ (<80 GPa) and a Princeton Instrument SpectraPro PIX-400BR spectrometer (>80 GPa) before and after the experiment. The P uncertainty is estimated from the fluorescence measurements of different ruby spheres. The P uncertainty is relatively small up to 103(3) GPa, which suggests that the sample chambers were under a relatively hydrostatic condition. We used 50° forward symmetric scattering geometry. Under symmetric scattering geometry, the measured velocities (V) are independent of the refractive index of the measured material and thus can be calculated directly from the Brillouin frequency shift ($\Delta\varpi$)

$$V = \frac{\Delta\varpi\lambda_0}{2\sin(\theta/2)}, \quad (1)$$

where λ_0 is the wavelength of the incoming laser, and θ is the external scattering angle between the incoming and scattered light. The scattering angle θ is calibrated to be $50.37(5)^\circ$ using a standard silica glass 7980 (Corning Inc.) which has been precisely measured using gigahertz ultrasonic interferometry.[23,24] The scattering angle uncertainty of 0.05° propagates to a velocity uncertainty of $\sim$0.1%, which is within the $\sim$20 m/s resolution limit of Brillouin spectroscopy. The two single-crystal diamond anvils are orientated in a way that the fast and slow directions matched each other for the high-P measurements of ice due to the overlap between the Vp of ice and the Vs of diamond at $P > \sim$45 GPa.

In this study, we did not use single-crystal Brillouin spectroscopy to obtain the individual elastic moduli of high-P ice.[25] The single-crystal ice sample tends to break down and form polycrystalline aggregates at high-P conditions.[25] Ice VII and ice X are both crystallographically cubic,[16] and thus, the maximum and minimum velocities values are directly linked to the single-crystal elastic moduli C_{ij} and the density ρ by the following equations:
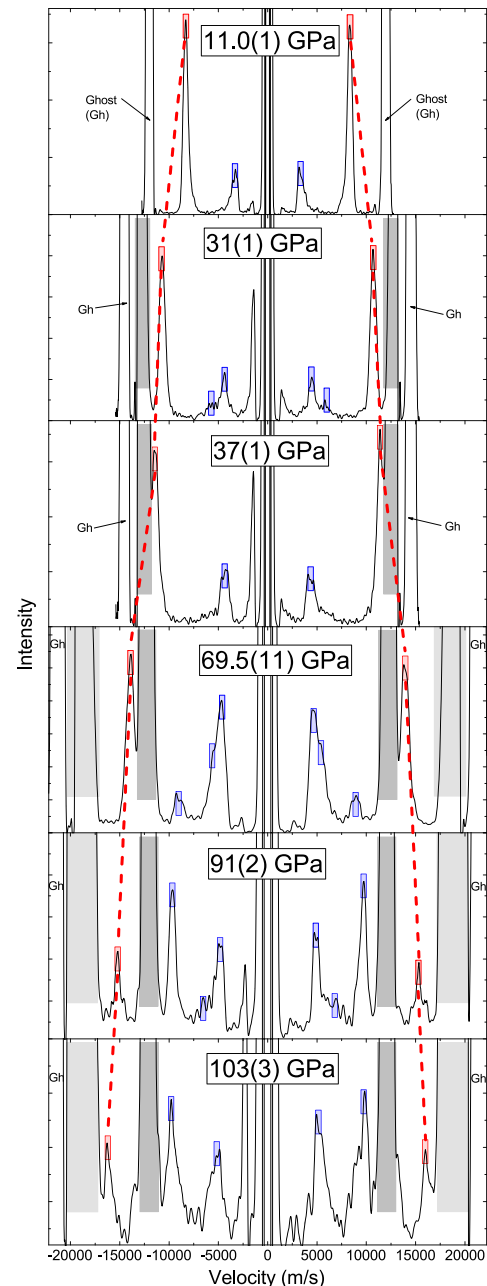
$$Vs_{max} = (C_{44}/\rho)^{1/2}, \quad (2)$$

$$Vs_{min} = [(C_{11} - C_{12})/2\rho]^{1/2}, \quad (3)$$

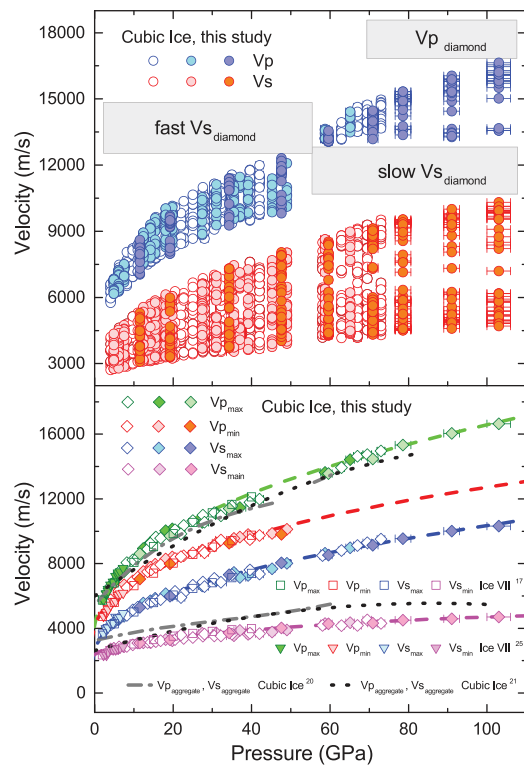$$Vp_{max} = [(C_{11} + 2C_{12} + 4C_{44})/3\rho]^{1/2}, \quad (4)$$

$$Vp_{min} = (C_{11}/\rho)^{1/2}. \quad (5)$$

Therefore, we can perform multiple measurements to obtain the maximum and minimum Vp and Vs values at each P to invert the best-fit density-normalized single-crystal elastic moduli C_{ij}/ρ of the cubic high-P ice polymorphs. In this study, for each P, the Brillouin measurements have been made at a minimum of 4 different azimuthal angles. At each angle, we also made multiple measurements at different sample positions (supplementary material, Table S1). Typical Brillouin spectra at a number of different P values are shown in Fig. 1. All spectra are with an excellent signal to noise ratio. To ensure better sampling of the DAC sample, we have made between 8 and 33 measurements at various sample positions and directions within the sample capsule at each P (Fig. 2, supplementary material, Table S1). This

FIG. 1. Typical Brillouin spectra of ice at different pressures. Gh represents the ghost peak on the size of the Brillouin spectra. The light gray and gray areas represent the Vp and Vs values of the diamond anvil, and red and blue squares indicate the Vp and Vs values of ice.

approach was used previously to determine the single-crystal elastic properties of ice VII up to 40 GPa.[17] However, if the high-P ice became polycrystalline and fine-grained within the DAC sample chamber, broad Vp and Vs peaks with large Full-Width-Half-Maximum (FWHM) values would show up in the obtained Brillouin spectrum. In such a case, identifying the velocity extremums is difficult, and the
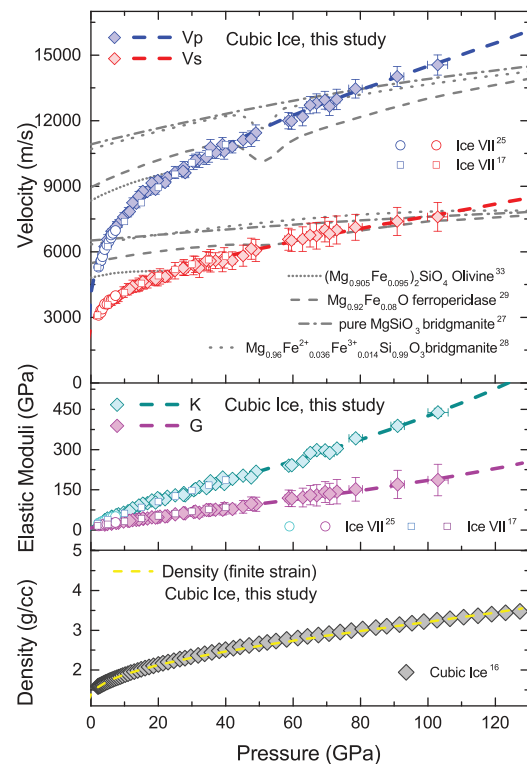
FIG. 2. All the measured Vp, Vs, Vp_{max}, Vs_{max}, Vp_{min}, and Vs_{min} of ice at high-P conditions. The values obtained from the previous studies are shown in gray dash-dotted lines,[20] black dotted lines,[21] open squares,[17] and down-pointed triangles[25] in the bottom plot.

calculated single-crystal elastic moduli values could be misleading. Therefore, in this study, long-time thermal annealing was employed to encourage crystal growth, and sharp peaks with small FWHM were observed within the entire P range (Fig. 1). Most of the Brillouin spectra obtained in this study were collected from one or a few large ice single crystals. When $30\,GPa < P < 45\,GPa$, all measurements were performed along the 4 directions where the Vs of single-crystal diamond anvils reached the maximum. When $P > 55\,GPa$, the measurements were performed along the 4 minimum Vs directions of diamond anvils. Over the entire measured P range, Vp of ice showed an increasing trend with P, as indicated by the red dashed lines in Fig. 1. Sometimes, multiple shear modes were observed, as shown by the blue rectangles in Fig. 1. It is worth noting that at 69.5(9) GPa, the Vp of ice clearly exceeds the Vs of diamond (indicated by the gray shaded area) and eventually approaches the Vp of diamond (light gray shaded area) at the highest measured P of 103(3) GPa. All the obtained velocities are plotted in Fig. 2.

Based on the best-fit density-normalized single-crystal elastic moduli C_{ij}/ρ of the cubic ice polymorphs at high-P conditions, we subsequently calculated the isotropic aggregate velocities of polycrystalline ice based on Voigt-Reuss-Hill average (supplementary material, Table S2). Due to the unquenchable nature of ice VII and X, a finite-strain approach was used to fit the obtained P-Vp-Vs dataset with fixed $\rho = 1.6747$, $Ks = 37(2)$ GPa, and $G = 21(1)$ GPa at the lowest P 4.1

GPa.[16] The calculated high-P ρ values based on the finite strain theory agree well with the ρ measured by X-ray diffraction up to 128 GPa,[16] further ensuring the robustness of our approach (Fig. 3). The P derivatives of the adiabatic bulk (Ks) and shear (G) modulus are calculated as $Ks_{(4.1\,GPa)}' = 5.3(2)$, $G_{(4.1\,GPa)}' = 2.2(1)$, $Ks_{(4.1\,GPa)}'' = -0.30(5)$, and $G_{(4.1\,GPa)}'' = -0.13(3)$. The single-crystal C_{ij} values and their P derivatives were calculated lastly: $C_{11(4.1\,GPa)} = 54(2)$ GPa, $C_{11(4.1\,GPa)}' = 6.17(8)$, $C_{11(4.1\,GPa)}'' = -0.265(6)$ GPa^{-1}, $C_{44(4.1\,GPa)} = 29(2)$ GPa, $C_{44(4.1\,GPa)}' = 3.79(7)$, $C_{44(4.1\,GPa)}'' = -0.152(5)$ GPa^{-1}, $C_{12(4.1\,GPa)} = 28(3)$ GPa, $C_{12(4.1\,GPa)}' = 4.39(9)$, and $C_{12(4.1\,GPa)}'' = -0.174(8)$ GPa^{-1}. The detailed data analysis procedure and results can be found in the supplementary material (Text S1, Table S2).

All measured Vp, Vs, and the extremum velocities at all P values are plotted in Fig. 2. We have not observed any clear discontinuities beyond experimental uncertainties [∼5% at 103(3) GPa]. Ice VII and ice X are indistinguishable from the sound velocity data presented in this study. Our experimentally determined velocity extremum agrees well with the previous single-crystal elasticity studies up to 7.3 GPa[25] and 40 GPa.[17] On the other hand, the Vp and Vs values obtained from previous polycrystalline sound velocity measurements are within the extremum bonds yet approaching Vp_{max} and Vs_{min} at high P values, as shown by the gray dash-dotted and black dotted lines in Fig. 2.[20,21] Ice VII crystals may form lattice-preferred orientation (LPO) at high-P conditions,[5] and thus, previous polycrystalline studies might suffer

FIG. 3. Aggregate elastic properties and densities of ice at high-P conditions. Comparison with previous studies of high-P silicates are shown in gray dashed,[29] dotted,[28] shot dotted,[33] and dash-dotted[27] lines. Previous measurements on ice are plotted with open circles,[25] open squares,[17] and gray diamonds.[16]
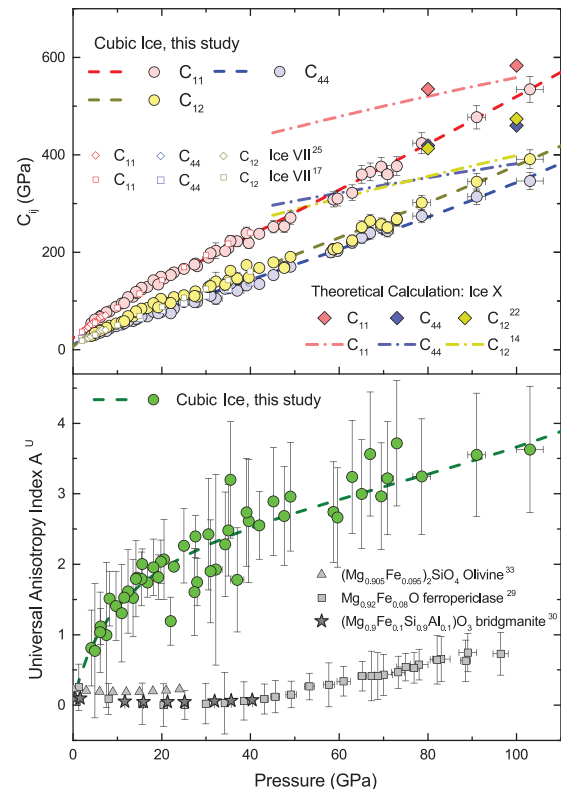
from the limited sampling of the sample inside the DAC, and the obtained values could not represent the true homogeneous isotropic velocities of polycrystalline ice under high-P conditions.

The aggregate Vp, Vs, Ks, G, and ρ values obtained from this study are plotted against P in Fig. 3. Our experimentally determined Vp, Vs, Ks, and G agree well with the previous single-crystal studies up to 7.3 GPa[25] and 40 GPa.[17] The close to linear P dependence of the Ks and G implies a significant increase in the incompressibility and hardness of ice at high P values. This type of mechanical behavior is commonly observed for silicates and super hard materials, such as diamond,[26] and is not expected for high-P ice. Compared with the high-P mineral phases that are expected to exist in deep terrestrial planetary bodies, the Vp and Vs values of the cubic ice high-P polymorphs exceed those of ferropericlase and bridgmanite between 40 and 60 GPa and 80 and 100 GPa,[27–30] respectively (Fig. 3). In the terrestrial planetary bodies, although ice is significantly buoyant compared with the high-P silicates, counter-intuitively, as a volatile phase, polycrystalline ice's isotropic sound velocities can actually be comparable to or even faster than high-P silicates at high-P conditions (Fig. 2).

As shown in Fig. 4, similar to Ks and G, C_{ij} values also show the close to linear P dependence. Comparing the single-crystal C_{ij} values determined in this study with previous studies, our results matched the single-crystal elasticity measurements of ice VII very well.[17,25] Compared with the theoretical calculation results of ice X,[14,22] our obtained single-crystal elasticity models disagree with the theoretical predictions at P values lower than 100 GPa. However, the C_{ij} values at the highest P 103(3) GPa clearly approach the predicted C_{ij} values of ice X,[14] although no abrupt change is observed in the explored P range. The ice VII–X transition might be a continuous gradual phase transition and probably have no measurable effects on the mechanical properties of high-P ice. We also calculated the universal elastic anisotropy index[31] A^U of high-P cubic ice up to Mbar P (supplementary material, Table S2). It is about a factor of 5–10 higher than the terrestrial high-P silicates ferropericlase and bridgmanite (Fig. 4). The A^U of ice quickly increased to 1.7–1.9 at 14–16 GPa and then follow a more gradual increasing trend at higher P. The change of A^U at ~14–16 GPa coincides with a previously reported transition of the cubic ice VII into an intermediate tetragonally distorted structure,[32] although further studies are needed to clarify this issue. The absolute Vp and Vs azimuthal anisotropy of ice reaches 27% and 74% at ~100 GPa, which are much higher than those of any major mantle silicate minerals[29,30,33] and comparable to those of the extremely anisotropic serpentine minerals at ambient conditions.[34]

Many icy planets and satellites in the solar system are believed to have active tectonic systems. For example, in addition to the dilational bands (analog to the midocean-ridges on the Earth's surface) that create new surfaces on Europa,[6] a recent study using Galileo spacecraft images suggested that the ongoing subduction processes are currently recycling the ice shell on the surface into Europa's interior.[3] Long-term cooling induced thermal volume contraction could also deform the icy lithosphere of Titan and produce the mountain belts on its surface, which were observed by Cassini Radar instrument.[4] Moreover, recent planetary simulations revealed the important role of the high-P ice polymorphs in the internal dynamics in the water-rich "super-Earth" exoplanets.[1] Therefore, the carefully constrained elastic properties of high-P ice in this study are crucial for studying the tectonic activities and convection in the icy planetary interiors. In the terrestrial planetary bodies, due to its extreme elastic anisotropy, the presence of

FIG. 4. Single-crystal elastic moduli C_{ij} and universal elastic anisotropy index A^U of cubic ice at high-P conditions. Previous measurements of ice VII are shown by open squares[25] and open diamonds.[17] Theoretical calculations of ice X are shown by dash-dotted lines[14] and diamonds.[22] The A^U values of high-P silicates are plotted with gray squares,[29] stars,[30] and triangles[33] for comparison in the bottom plot.

even a very small amount of ice can lead to observable anisotropic signatures, whereas the isotropic aggregate velocities are likely to show close to neutral or even positive anomalies when co-existing with other silicates, such as olivine, bridgmanite, and ferropericlase. A recent seismic study by Li et al.[35] suggested that the nondouble-couple radiation pattern of the deep earthquakes could be explained by the extremely large Vs anisotropy of ~25% near the earthquake generation zone in subducting slabs. Such strong anisotropy is impossible to be caused by the lattice-preferred orientation (LPO) of major upper mantle minerals such as olivine and wadsleyite.[33] Based upon the measurements in this study, due to the extraordinary high intrinsic anisotropy and the small bulk and shear moduli of ice VII, the 25% Vs anisotropy can also be easily explained by either the LPO or shape preferred orientation of ice VII buried within the subducting slabs.

See the supplementary material for the detailed data analysis procedure, experimental system layout, numerical experimental data, and calculated elastic moduli at each P.

REFERENCES

[1] R. Fu, R. J. O'Connell, and D. D. Sasselov, Astrophys. J. **708**, 1326 (2010).

[2] R. Redmer, T. R. Mattsson, N. Nettelmann, and M. French, Icarus **211**, 798 (2011).

[3] S. A. Kattenhorn and L. M. Prockter, Nat. Geosci. **7**, 762 (2014).

[4] G. Mitri, M. T. Bland, A. P. Showman, J. Radebaugh, B. Stiles, R. Lopes, J. I. Lunine, and R. T. Pappalardo, J. Geophys. Res.: Planets **115**, E10002, https://doi.org/10.1029/2010JE003592 (2010).

[5] J. P. Poirier, Nature **299**, 683 (1982).

[6] L. M. Prockter, J. W. Head, R. T. Pappalardo, R. J. Sullivan, A. E. Clifton, B. Giese, R. Wagner, and G. Neukum, J. Geophys. Res. **107**, 4-1, https://doi.org/10.1029/2000JE001458 (2002).

[7] C. R. Bina and A. Navrotsky, Nature **408**, 844 (2000).

[8] A. F. Goncharov, C. Sanloup, N. Goldman, J. C. Crowhurst, S. Bastea, W. M. Howard, L. E. Fried, N. Guignot, M. Mezouar, and Y. Meng, J. Chem. Phys. **130**, 124514 (2009).

[9] T. Bartels-Rausch, V. Bergeron, J. H. Cartwright, R. Escribano, J. L. Finney, H. Grothe, P. J. Gutiérrez, J. Haapala, W. F. Kuhs, J. B. Pettersson, and S. D. Price, Rev. Mod. Phys. **84**, 885 (2012).

[10] K. R. Hirsch and W. B. Holzapfel, Phys. Lett. A **101**, 142 (1984).

[11] E. Sugimura, T. Komabayashi, K. Ohta, K. Hirose, Y. Ohishi, and L. S. Dubrovinsky, J. Chem. Phys. **137**, 194505 (2012).

[12] A. F. Goncharov, V. V. Struzhkin, M. S. Somayazulu, R. J. Hemley, and H. K. Mao, Science **273**, 218 (1996).

[13] E. Sugimura, T. Iitaka, K. Hirose, K. Kawamura, N. Sata, and Y. Ohishi, Phys. Rev. B **77**, 214103 (2008).

[14] M. Kuriakose, S. Raetz, Q. M. Hu, S. M. Nikitin, N. Chigarev, V. Tournat, A. Bulou, A. Lomonosov, P. Djemia, V. E. Gusev, and A. Zerr, Phys. Rev. B **96**, 134122 (2017).

[15] A. Polian and M. Grimsditch, Phys. Rev. Lett. **52**, 1312 (1984).

[16] R. J. Hemley, A. P. Jephcoat, H. K. Mao, C. S. Zha, L. W. Finger, and D. E. Cox, Nature **330**, 737 (1987).

[17] C. S. Zha, H. K. Mao, R. J. Hemley, and T. S. Duffy, Rev. High Pressure Sci. Technol. **7**, 739 (1998).

[18] C. S. Zha, R. J. Hemley, S. A. Gramsch, H. K. Mao, and W. A. Bassett, J. Chem. Phys. **126**, 074506 (2007).

[19] M. Somayazulu, J. Shu, C. S. Zha, A. F. Goncharov, O. Tschauner, H. K. Mao, and R. J. Hemley, J. Chem. Phys. **128**, 064510 (2008).

[20] Y. Asahara, K. Hirose, Y. Ohishi, N. Hirao, and M. Murakami, Earth Planet. Sci. Lett. **299**, 474 (2010).

[21] M. Ahart, M. Somayazulu, S. A. Gramsch, R. Boehler, H. K. Mao, and R. J. Hemley, J. Chem. Phys. **134**, 124517 (2011).

[22] B. Journaux, R. Caracas, P. Carrez, K. Gouriet, P. Cordier, and I. Daniel, Phys. Earth Planet. Inter. **236**, 10 (2014).

[23] J. S. Zhang, J. D. Bass, T. Taniguchi, A. F. Goncharov, Y. Y. Chang, and S. D. Jacobsen, J. Appl. Phys. **109**, 063521 (2011).

[24] J. S. Zhang, J. D. Bass, and G. Zhu, Rev. Sci. Instrum. **86**, 063905 (2015).

[25] H. Shimizu, T. Nabetani, T. Nishiba, and S. Sasaki, Phys. Rev. B **53**, 6107 (1996).

[26] F. Occelli, P. Loubeyre, and R. LeToullec, Nat. Mater. **2**, 151 (2003).

[27] M. Murakami, S. V. Sinogeikin, J. D. Bass, N. Sata, Y. Ohishi, and K. Hirose, Earth Planet. Sci. Lett. **259**, 18–23 (2007).

[28] S. Fu, J. Yang, Y. Zhang, T. Okuchi, C. McCammon, H. I. Kim, S. K. Lee, and J. F. Lin, Geophys. Res. Lett. **45**, 4725, https://doi.org/10.1029/2018GL077764 (2018).

[29] J. Yang, X. Tong, J. F. Lin, T. Okuchi, and N. Tomioka, Sci. Rep. **5**, 17188 (2015).

[30] A. Kurnosov, H. Marquardt, D. J. Frost, T. B. Ballaran, and L. Ziberna, Nature **543**, 543 (2017).

[31] S. I. Ranganathan and M. Ostoja-Starzewski, Phys. Rev. Lett. **101**, 055504 (2008).

[32] E. Wolanin, P. Pruzan, J. C. Chervin, B. Canny, M. Gauthier, D. Häusermann, and M. Hanfland, Phys. Rev. B **56**, 5781 (1997).

[33] J. S. Zhang, J. D. Bass, and B. Schmandt, J. Geophys. Res. Solid Earth **123**, 2674, https://doi.org/10.1002/2017JB015339 (2018).

[34] L. Bezacier, B. Reynard, J. D. Bass, C. Sanchez-Valle, and B. Van de Moortèle, Earth Planet. Sci. Lett. **289**, 198 (2010).

[35] J. Li, Y. Zheng, L. Thomsen, T. J. Lapen, and X. Fang, Nat Geosci. **11**, 696 (2018).